Disturbance observer based Control Design of Flapping-wing MAV Considering Model Uncertainties

Inrae Kim[1], Heetae Park[1], Seungkeun Kim[1]*, Jinyoung Suk[1] and Sungbong Cho[2]
[1]Department of Aerospace Engineering, Chungnam National University, Daejeon, 34134, Republic of Korea
[2]Agency for Defence Development, Daejeon, 34186, Republic of Korea

ABSTRACT

This paper presents controller design for the stable flight of Flapping-Wing Micro Aerial Vehicle (FWMAV). FWMAV has model uncertainty in aerodynamics and vehicle dynamics generated by the flapping wing motions. Hence, for the robust controller design, disturbance observer-based controller (DOBC) is designed considering these model uncertainties as system disturbance. Dynamic modeling takes into account flapping wing kinematics, aerodynamics, and 6DoF dynamics. Finally, to verify the performance of the applied controller, numerical simulations are performed in a MATLAB environment in hovering flight condition, and the result of disturbance observer based controller is analyzed.

1 INTRODUCTION

In recent decades, unmanned aerial vehicle (UAV) have experienced rapid development. Micro air vehicle (MAV) is a class of UAVs restricted in size and has been tackled through biomimetic technology mimicking insects [1, 2, 3]. This is because insects can be highly maneuverable and have stable hovering and excellent aerodynamic characteristics unlike fixed-wing and rotary-wing aircraft. This feature can effectively help MAVs perform a variety of missions, including surveillance, reconnaissance, secret infiltration, and search inside a collapsed building. Also, it would be advantageous to swarm flight in the future.

Especially, aerodynamic analysis for flapping in the area of low Reynolds number, actuator, micro sensor, battery, etc, the research are still studying for micro miniaturization in the actual making as well as the theoretical and analytical aspects. For most of the MAV's study, it was carrying out experiments by using the external power supply. State variables of the MAV are measured from the outside because of the weight limit. Then, the measured value was used to study the attitude control from the outside [4]. The attitude control of MAV is very necessary for excellent performance. So, a lot of simulation was conducted for attitude control over the world.

*Corresponding Author: skim78@cnu.ac.kr

In Ref. [5], the study for a variety of input control was conducted about flapping frequency or phase using pitch attitude change by flapping motion. Ref. [6] presented key aspects of active flexible wing technique. Cheng and Deng [7] proposed a mathematical model of near-hover attitude dynamics and control in flapping flight. Study of insect mimicking is more focus on modeling than control. But, these MAV attitude control is essential to basic techniques for the design and production and system development in future. Many people have been trying to solve control problems in a variety of fields, so that more advanced control design techniques was announced as a result of these efforts. However, despite these recent research, actually, PID controller is still the most. Among other reasons, because PID is relatively easy to design a controller, good and economic effects. Disturbance observer for similar reasons has been used much since the late 1980s. The DOB scheme which is a kind of more straightforward and efficient disturbance suppression mechanism is developed by [8] To date, research was conducted about DOB. There is a study that applies to difficult non-linear and complex system. Nevertheless, a strong disturbance removal performance shows a simple feature. The DOB control system had been successfully applied to many fields and proved to be an effective countermeasure against the disturbance. Through these advantages, apply to FWMAV.

The overall structure of this paper is given as follows. Section 2 introduces a mathematical model of FWMAV, which combines quasi-steady aerodynamics and rigid body dynamics. Section 3 proposes the flapping flight control based on the PID controller and Track guidance, and additional disturbance observer based control. Section 4 presents a numerical simulation environment and results of FWMAV waypoint flight. Last, conclusions and future work are given in section 5.

2 MATHEMATICAL MODELING

2.1 Coordinate system

This paper uses four coordinate frames to describe flapping kinematics and body dynamics as shown in Fig. 1: 1) E : Earth-fixed frame, a fixed coordinate system on the Earth's surface; 2) B : Body-fixed frame, fixed coordinates to the center of gravity for a vehicle; 3) S : Stroke-plane frame, fixed coordinates to each connecting point between each wing and a body; and 4) W : Wing-fixed frame, fixed coordinates to the center of pressure for each wing.

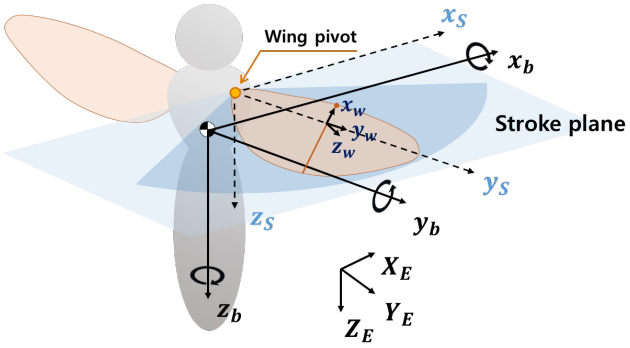

Figure 1: Coordinate system of FWMAV

2.2 *Flapping wing kinematics*

The motion of the flapping wing can be defined with three independent angular degrees of freedom at the wing base pivot as shown in 'Figure 3': 1) ϕ : Stroke angle, back and forth motion of the wing; 2) θ : Deviation angle, up and down motion of the wing with respect to the stroke plane; and 3) ψ : Feathering angle, the geometrical angle of attack of the wing surface.

FWMAV is flying by the force generated by the flapping motion. Actual insect flapping motion has different complicated motion depending on the type and size of insects [9]. In fact, it is difficult to apply real insects flapping motion to FWMAV. Therefore, this paper considers simple flapping. Based on this wing kinematics definition, the motion of each rotational degree of freedom is defined with a sinusoidal function, to reproduce the periodic wing beat motion of the flapping flight, 'Equation 1 to 4' show the wing kinematics function for each rotational degree of freedom :

$$\phi(t) = \phi_{amp} \cos(2\pi f t) + \bar{\phi} \tag{1}$$

$$\psi(t) = \frac{\psi_{amp}}{\tanh(C_\alpha)} \tanh\left(C_\alpha \sin(2\pi f t) + \frac{\pi}{2}\right) + \bar{\psi} \tag{2}$$

$$\alpha(t) = \frac{\pi}{2} - sign(\dot{\phi})\psi \tag{3}$$

$$\theta(t) = 0 \tag{4}$$

where t is time, f is the typical flapping frequency of FWMAV, and C_α is a coefficient for adjusting the interval of the stroke reversal. Each kinematics function has two variables, which are the amplitude and bias. The angle of attack(α) can be expressed as 'Equation 3' and the value of the angle of attack is determined according to the sign of $\dot{\phi}$.

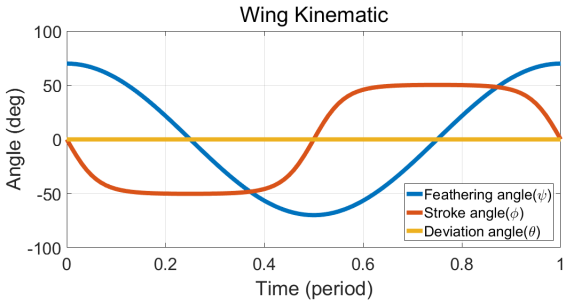

Figure 2: Amplitude of the wing kinematics

2.3 *Flapping flight aerodynamics*

The aerodynamic forces generated by the wings are complex and the motion changes rapidly in low Reynolds number flows. In the absence of skin friction, the instantaneous forces generated by a thin, flapping wing may be represented as the sum of four force components, each acting normal to the wing surface :

$$F_{total} = F_{trans} + F_{rot} + F_{add} + F_{wc} \tag{5}$$

where F_{trans} is the instantaneous translational force, F_{rot} is the rotational force, F_{add} is the force due to the inertia of the added mass of the fluid and F_{wc} is the force due to wake capture. Among the four major aerodynamic components, the aerodynamics generated from a translational and a rotational motion of the wing is modeled for this study [10, 11]. The wake capture effect is neglected because the inherent unsteadiness of the phenomenon makes it hard to be modeled with a quasi-steady approach. The instantaneous translational and rotational forces from each aerodynamic strip are calculated by

$$\begin{aligned} F_{tr,T} &= \tfrac{1}{2}\rho A_w C_T U_{cp}^2 \\ F_{tr,N} &= \tfrac{1}{2}\rho A_w C_N U_{cp}^2 \end{aligned} \tag{6}$$

where U_{cp} is the velocity of the wing at the center of pressure. In small advance ratio, this parameter can be defined as :

$$U_{cp} = \hat{r_2} L \dot{\phi} \tag{7}$$

In which $\hat{r_2}$ is the normalized distance of center of pressure from wing base :

$$\hat{r_2}^2 = \frac{\int_0^L c(r) r^2 dr}{L^2 A_w} \tag{8}$$

where ρ is the air density, A_w is the wing area, L us the wing length, $\dot{psi}$ is stroke velocity, and c is wing chord width. C_N and C_T are the force coefficient each Normal, tangential. This force coefficient for the model wing was measured in [3] and fitted with the following equation :

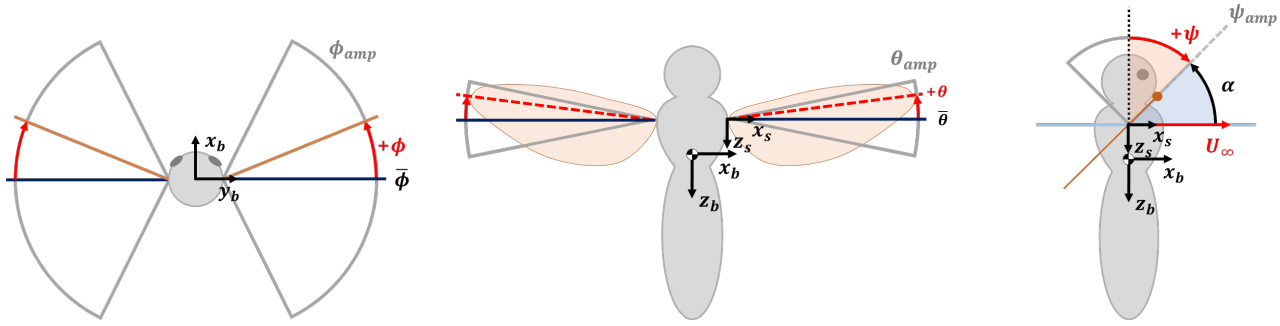

(a) Stroke angle ϕ (top view)

(b) Deviation angle θ (back view)

(c) Feathering angle ψ (side view)

Figure 3: Wing Kinematics

$$C_N = 3.4 \sin\alpha$$
$$C_T = \begin{cases} 0.4\cos^2(2\alpha) & 0° < \alpha < 45° \\ 0 & otherwise \end{cases} \quad (9)$$

α stands for the angle of attack. A quasi-steady treatment of the aerodynamic force due to wing rotation, $F_{rot,N}$, was calculated by [12] :

$$F_{rot,N} = \frac{1}{2}\rho A_w C_{rot} \hat{c} c_m \dot{\alpha} U_{cp} \quad (10)$$

where C_{rot} is the theoretical value of rotational coefficient, $\hat{c} = c/\bar{c}$ is the normalized chord length, and c_m is the maximum wing chord width. then C_{rot} and $\hat{c}$ is given by :

$$C_{rot} = 2\pi(0.75 - \hat{x_0}) \quad (11)$$

$$\hat{c} = \frac{\int_0^L c^2(r)rdr}{\hat{r_2} L A_w c_m} \quad (12)$$

$\hat{x_0}$ is the dimensionless distance of the longitudinal rotation axis from the leading edge. Therefore, the total lift and drag forces are computed as follow :

$$F_N = F_{tr,N} + F_{rot,N}$$
$$F_T = F_{tr,N} \quad (13)$$

$$F_L = F_N \cos\alpha + F_T \sin\alpha$$
$$F_D = -F_N \sin\alpha - F_T \cos\alpha \quad (14)$$

2.4 *Body dynamics*

The dynamics of the FWMAV can be described, under rigid body assumption, by Newton-Euler motion equations. Similar to an aircraft we obtain 12 ordinary differential equations with 12 unknown coordinates.

Force equations.

$$\dot{u} = rv - qw + g_x + a_x$$
$$\dot{v} = pw - ru + g_y + a_y \quad (15)$$
$$\dot{w} = qu - pv + g_z + a_z$$

where

$$g_x = -g\sin\theta$$
$$g_y = g\sin\phi\cos\theta \quad (16)$$
$$g_z = g\cos\phi\cos\theta$$

Here, $[u, v, w]$ denotes the body-axis velocities, $[p, q, r]$ indicates the body-axis angular velocities, $[\phi, \theta, \psi]$ is the Euler angles from navigation to body frame, and g is the acceleration of gravity. Moreover, $[a_x, a_y, a_z]$ include all the airframe loads from aerodynamics, propulsion, and winds [13].

Moment equations.

$$\dot{p} = (c_1 r + c_2 p)q + c_3 L + c_4 N$$
$$\dot{q} = c_5 pr - c_6(p^2 - r^2) + c_7 M \quad (17)$$
$$\dot{r} = (c_8 p - c_2 r)q + c_4 L + c_9 N$$

where $[L, M, N]$ is moments with respect to the center of gravity. We define inertia coefficient c_1 to c_9 as 'APPENDIX A'

$$\begin{bmatrix} mI & 0 \\ 0 & I_b \end{bmatrix} \begin{bmatrix} \dot{v_b} \\ \dot{w_b} \end{bmatrix} + \begin{bmatrix} w_b \times m v_b \\ w_b \times I_b w_b \end{bmatrix} = \begin{bmatrix} \Sigma F \\ \Sigma M \end{bmatrix} \quad (18)$$

where m is the mass of the FWMAV, I_b is the inertia matrix relative to the center of mass, I is the the 3×3 identity matrix, and v_b and w_b are the linear and angular velocity vectors in body frame coordinates [3, 14]. Since the lift and drag forces are given by 'Equation14' are calculated relative to the Stroke-plane frame, a coordinate transformation is necessary before obtaining the forces and torques acting on the body frame.

$$\begin{bmatrix} F_a \\ M_a \end{bmatrix} = R_{sb} \begin{bmatrix} F_{a,S} \\ M_{a,S} \end{bmatrix} \quad (19)$$

where R_{sb} is the rotation matrix of the body frame relative to the stroke plane, $F_{a,S}$, and $M_{a,S}$ are the aerodynamic force and moment generated in the stroke-plane frame and F_a and M_a are the aerodynamic force and moment in the body frame. Given the lift and drag generated by aerodynamics, together with the stroke angle, the forces and torques in the stroke plane can be calculated as

$$F_{a,S} = \begin{bmatrix} -F_{D,l}\cos\phi_l - F_{D,r}\cos\phi_r \\ -F_{D,l}\sin\phi_l + F_{D,r}\sin\phi_r \\ -F_{L,l} + F_{L,r} \end{bmatrix} \tag{20}$$

$$M_{a,S} = \hat{r_2}L \begin{bmatrix} F_{L,l}\cos\phi_l - F_{L,r}\cos\phi_r \\ F_{L,l}\sin\phi_l + F_{L,r}\sin\phi_r \\ -F_{D,l} + F_{D,r} \end{bmatrix} \tag{21}$$

These forces and moments are time-varying nonlinear equations for the flapping motion.

3 Flapping Flight Control

3.1 Control parameters

To perform attitude and position control, force and moment must be generated for each axis. Many universities abroad have generated moments in different ways and have chosen appropriate forms for each study [1, 15]. In this study, the force and moment generation method that can implement FWMAV is selected from among them and it is shown in 'Figure 4' [16].

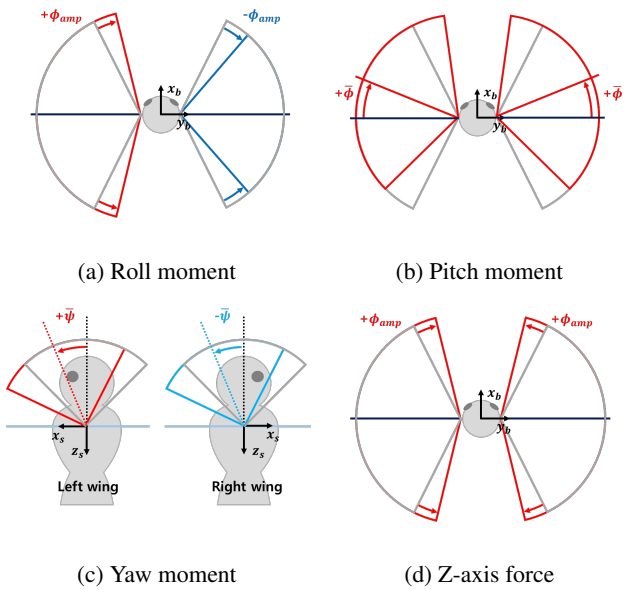

(a) Roll moment (b) Pitch moment

(c) Yaw moment (d) Z-axis force

Figure 4: Control force and moments generated through wing kinematics parameters

a) Roll moment is generated by giving a difference to the amplitude of the stroke angle of both wings; b) Pitch moment is generated by moving the center line of the stroke angle back and forth; c) Yaw moment is generated by moving the center line of the feathering angle in the opposite direction; , and d) Z-axis force is generated by giving a same amplitude of the stroke angle.

$$\phi(t) = (\phi_{amp} + \Delta\phi_{roll} + \phi_{hover})\cos(2\pi ft) + \phi_{pitch} + \bar{\phi} \tag{22}$$

$$\psi(t) = \frac{\psi_{amp}}{\tanh(C_\alpha)}\tanh\left(C_\alpha \sin(2\pi ft) + \frac{\pi}{2}\right) + \Delta\psi_{yaw} + \bar{\psi} \tag{23}$$

FWMAV use control inputs through flapping motion. 'Equation 22' is the Amplitude of the stroke angle is a control input variable and is used both as altitude, roll and pitch control. The flapping amplitude of one wing can be up to 180°. Therefore, the sum of the flapping amplitude control inputs must be limited to not exceed ±90°. The feathering angle is a control input variable for yaw control. The limit of this variable is determined by the forces that occur. In consideration of this, as shown in 'Table 1'.

Effect	Variable	Range
M_x	$\Delta\phi_{amp}$	$[-5°5°]$
M_y	$\bar{\phi}$	$[-5°5°]$
M_z	$\Delta\bar{\psi}$	$[-1°1°]$
F_z	ϕ_{amp}	$[-10°10°]$

Table 1: Range values of each control variable.

3.2 Attitude and position control

In this paper, PID(Proportional-Integral-Derivative) control is used for attitude and position control of the FWMAV. PID control is a classical automatic control technique that is most widely used in industrial control applications. Its design, implementation and tuning are simple since the design itself are response-based, it can be designed without knowledge of the system. In this study, a basic flight control system is designed as a multiple cascaded PID controller as shown in 'Figure 5'. Attitude controller is designed as an angular position and rate cascaded P-PID inner-outer loop structure to provide more stability and faster response due to rate feedback.

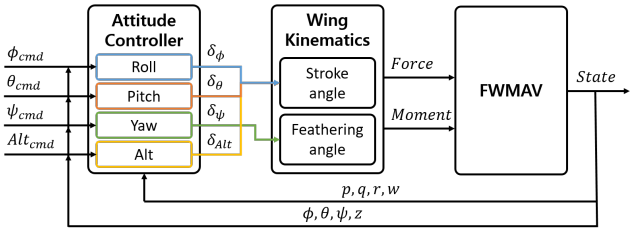

Figure 5: Schematic of the basic flight control system

3.3 Track Guidance

This section proposes a track guidance algorithm for efficient waypoint navigation of FWMAV. this paper assumes FWMAV flight conditions. 1) FWMAV is capable of hovering, but in case of waypoint flight, it makes a continuous flight with constant advance speed. 2) The heading of the vehicle coincides with the forward direction. And, track guidnance system is designed as shown in 'Figure 6'.

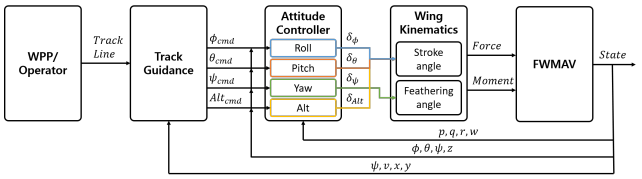

Figure 6: Structure of the track-guidance algorithm for FWMAV

When the waypoint of the FWMAV is determined, the algorithm of the track guidance has the following flow.

ALGORITHM

Input last and current waypoint position data

1: Caulculate the straight-line direction vector between the waypoints. (Track Heading)
2: Command the vehicle heading to match the Track heading. (ψ_{cmd})
3: Calculation of Cross track error Distance between Track and vehicle.
4: Determine the Cross track error sign code by the sign of ψ_d.
5: Instruction ϕ_{cmd} so that the value of Cross track error is 0.
6: When a vehicle enters the Waypoint Range, it moves to the next waypoint

First, calculate the heading angle from the previous waypoint to the current waypoint. This is called Track Heading. Next, ψ_{cmd} is created to match the heading of the FWMAV with the tracking heading. In this case, the heading is aligned with the Track direction, and then the command is generated to enter the Track. Since we know vehicle position and waypoint, we can calculate the Cross-track error distance, which is the vertical distance between vehicle and Track. At this time, the Cross-track error distance does not include sign information in the Track. Therefore, it is necessary to check whether the FWMAV is on the left or right side of the Track. In this paper, we calculate the angle between the track heading obtained above and the current waypoint. At this point, if ψ_d is positive, there is FWMAV on the right side of the Track if it is negative on the left side of the Track. After calculating distance and sign, ϕ_{cmd} is generated so that Cross track error becomes 0. Then, when the aircraft enters the predetermined waypoint range, it moves to the next waypoint.

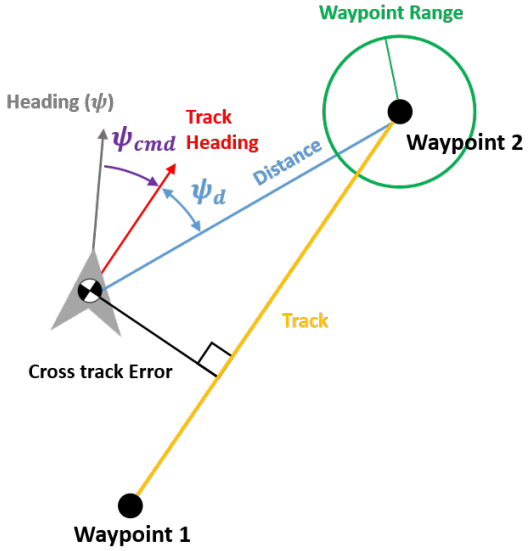

Figure 7: Track guidance algorithm for FWMAV

3.4 Disturbance observer based control

Disturbance generally exists in control systems and degrades performance or stability of the closed-loop system. Especially, aerial systems are subject to forces and moments caused by external wind and unmodeled dynamics due to complex aerodynamics. Thus, disturbance rejection is the major consideration for the control design of the aerial system to achieve safe flight. Disturbance observer implies various control technique that estimates disturbance in a broad sense. This study, Disturbance observer that uses the inverse of a nominal model is considered. This disturbance observer is an additional controller that can be designed separately from the outer loop controller design. In the concept of the disturbance observer, the disturbance does not only refer to the disturbance from the external environment but also uncertainties from the plant including unmodeled dynamics, parameter perturbations, and nonlinear couplings as a lumped disturbance.

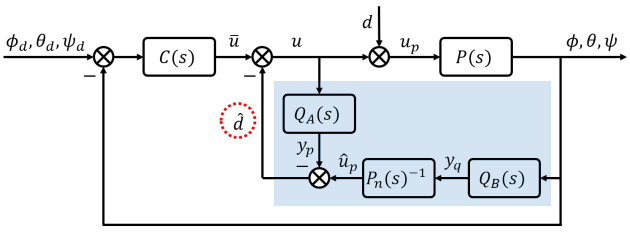

Figure 8: Disturbance observer control structure

Disturbance observer based control structure is shown in 'Figure 8'. $P(s)$ is the actual system with uncertainties,

ϕ_d,θ_d,ψ_d and u_p is input and output of the system, respectively. $C(s)$ is the outer loop controller. It is difficult to know the actual system $P(s)$ perfectly. However, the nominal model $P_n(s)$ can be seen. Therefore, if we know the output of the model and the control input, we can estimate the disturbance and compensate the disturbance controller. The implementation of Q-filter is to filter the noise and make an appropriate transfer function of $P_n(s)^{-1}$. The concept of the disturbance observer is to estimate the input to the system including disturbance (u_p) using the inverse of the nominal model($P_n(s)^{-1}$), and subtract the outer controller output (y_p); then it becomes the estimated disturbance ($\hat{d}$) as follows:

$$u = \bar{u} + y_p - \hat{u}_p = \bar{u} - \hat{d} \tag{24}$$

The desired dynamics of the system is considered as inertia-moment dynamics without friction. For example, Taking lateral dynamics can be simplified as follows :

$$L = J_{xx}\ddot{\phi} \tag{25}$$

$$L = c_t\delta_\phi - (J_{zz} - Jyy)\dot{\theta}\dot{\psi} \tag{26}$$

$$P_n(s) = \frac{\phi(s)}{\delta_\phi(s)} = \frac{1}{J_{xx}s^2} \tag{27}$$

Since a relative degree of the nominal plant is two, the minimum required the relative degree of the Q-filter is also two as:

$$Q_A(s) = Q_B(s) = \frac{a_0/\tau^2}{s^2 + (a_1/\tau)\,s + (a_0/\tau^2)} \tag{28}$$

where the coefficients (a_0 and a_1) of the Q-filter are chosen so that the following two expressions have negative real parts and that τ is small enough [17, 18].

4 Numerical Simulation

4.1 Simulation environment

This section carries out numerical simulations using the proposed controller, track guidance, and disturbance observer based control. The simulation works in MATLAB's Simulink. The simulation initial values were modeled by hummingbirds similar in size to the flapping-wing MAV with reference to various papers [19]. The detailed specifications are summarized in 'Table 2'.

The Simulation was performed under three conditions to verify the performance of the designed controller. At this time, the initial Euler angle and initial position in each environment are [0 0 0]. 1) Fly a diamond path in a non-disturbance environment. 2) Fly a diamond path without a disturbance observer in an environment where the north wind is blowing. 3) Diamond phth flight when a disturbance observer is used in a borehole environment.

Parameter	Value	Unit
ρ	1.225	kg/m^3
g	9.81	m/s^2
M	4.32e-3	kg
I_{xx}	4.92e-7	-
I_{yy}	5.57e-7	-
I_{zz}	4.11e-7	-
I_{xz}	2.2e-7	-
L	4.8e-2	m
$\hat{r_2}$	0.6	-
$\hat{x_0}$	0.25	-
c_m	1.9e-2	m
$\hat{c}$	0.6	-
A_w	6.11e-4	m^2
f	50	Hz
C_α	2.5	-
ϕ_{amp}	70	deg
ψ_{amp}	50	deg
$\bar{\phi}$	-3	deg
$\bar{\psi}$	0	deg

Table 2: Main parameter for simulation.

4.2 Simulation result

1. Non disturbance

'Figure 9a' shows the flight path of FWMAV. In the environment without disturbance, it can be confirmed that it follows well along the waypoint. Detailed position information can be found 'Figure 9b'. For X,Y position, the command value follows well. when the FWMAV reached the Waypoint range, the command changes to the next waypoint, and the algorithm works well. The Z position will overshoot but will follow the command value well. 'Figure 9c' compares the Euler angle command value with the vehicle Euler angle. It can be confirmed that ψ first follows the command value and becomes stable. θ has a constant value except when the waypoint is changed since the command value is generated so as to have a constant advancing direction. ϕ is repeatedly commanded to reduce the cross track error, and a "zig-zag" motion is generated by chattering around the track.

2. disturbance

This simulation includes disturbances. The disturbance assumed that the north wind was divided by a constant wind. The graph for the disturbance is shown in 'Figure 11'. The simulation environment is the same except for disturbance.

'Figure 11a' shows the flight path of the FWMAV in a disturbed environment. Compared to 'Figure 9a', it can be

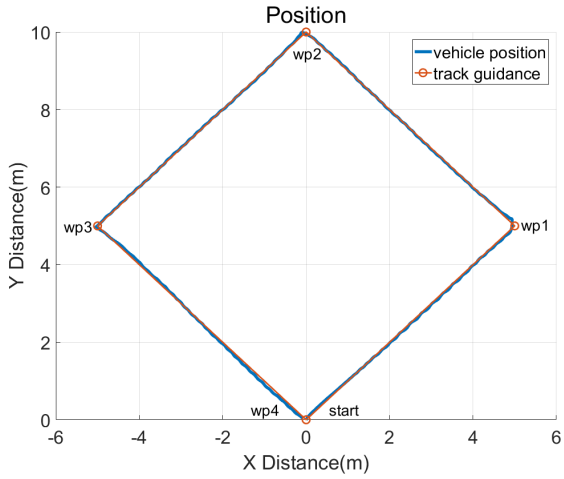

(a) FWMAV Path

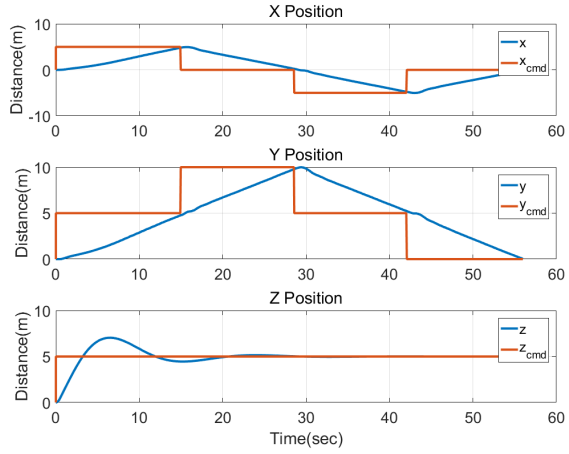

(b) Position command

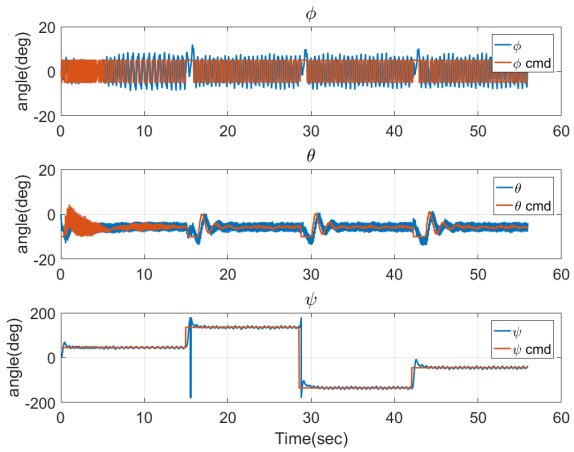

(c) Euler angle command

Figure 9: Simulation of non-disturbance

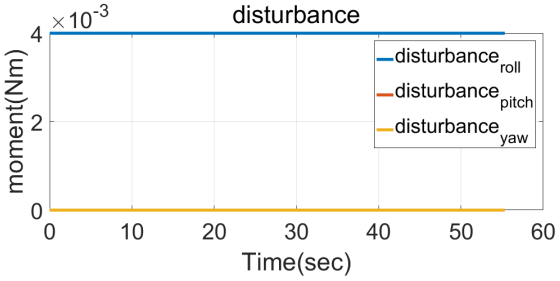

Figure 10: Disturbance

seen that it deviates much from the track, and it is far from the track around waypoint 1. The Euler angle can be confirmed by the fact that the track response is pushed by the wind and the command value response of ϕ and θ changes. In the case of ψ, the path of the track is constant, which is the same as when there is no disturbance.

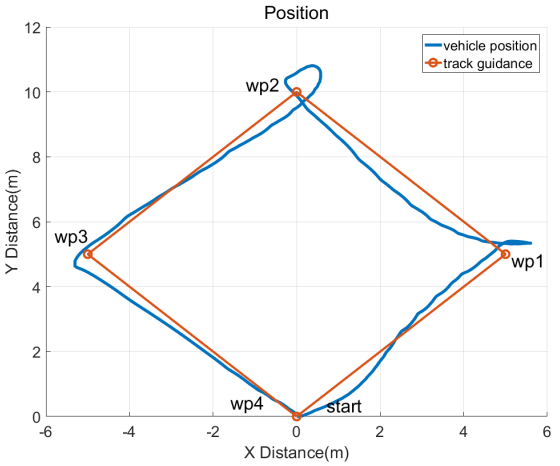

(a) FWMAV Path

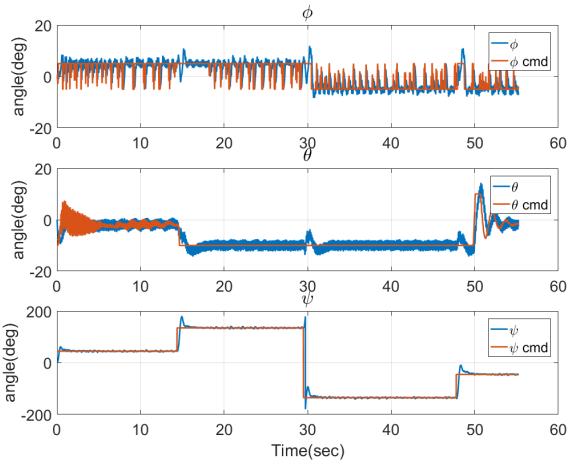

(b) Euler angle command

Figure 11: Simulation of disturbance

3. disturbance using DOBC

'Figure 12' is shows the simulation results using DOBC. 'Figure 12a' shows the flight path of the FWMAV, followed by a little more track than without the DOBC. Euler angle is similar to that of the absence of the DOBC, but it can be seen that the FWMAV's Euler angle is more stable. and the amplitude of the Euler angle is lowered and stabilized in the sections where overshoot occurs.

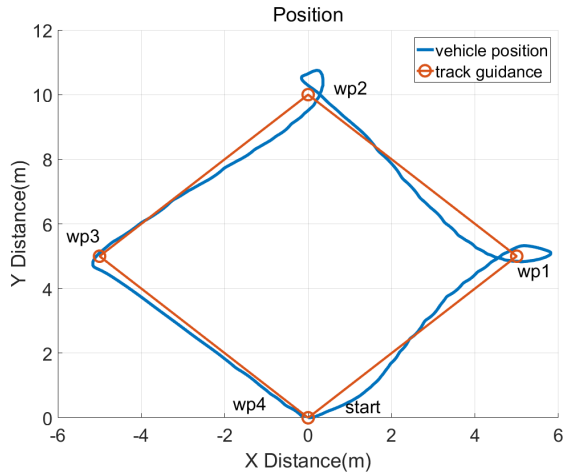

(a) FWMAV Path

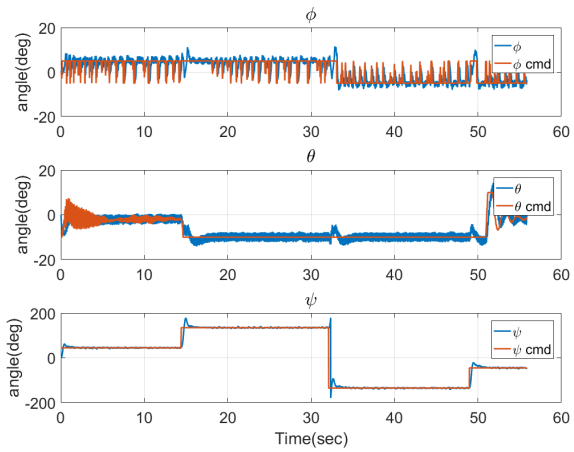

(b) Euler angle command

Figure 12: Simulation of disturbance with DOBC

5 Conclusion

In this paper, numerical modeling of the FWMAV is performed, implemented control variables, controller, and track guidance algorithm are designed. Numerical simulations were performed to verify the performance of waypoint flight in an environment with disturbance. Simulation results show that the FWMAV performed stable flight for a given waypoint in a non-disturbance environment. On the other hand, in the given environment of constant disturbance, it showed flight off the track, but the waypoint flight could be completed. We designed a disturbance observer to simulate a stable flight in a disturbance environment. As a result, the disturbance observer was able to follow the path well, but it showed a slight effect. Rather, it showed a good effect on stabilization of FWMAV's Euler angle. Simulation results show that there is a need to find a way to eliminate the chattering effect of the track guidance algorithm. As a result, unnecessary control command values are included, which can impair the control actuator in the real vehicle. In addition, the problem that the effect of the disturbance observer designed for stable flight in the disturbance environment was small will be complemented by the redesign of the disturbance observer. After completing the current simulation, we plan to model the actuator and sensor of the actual FWMAV in order to construct a simulated environment similar to the actual vehicle, and apply it to the simulation and analysis.

Acknowledgements

This research was supported by a grant to Bio-Mimetic Robot Research Center funded by Agency for Defense Development and Defense Acquisition Program Administration. (UD130070ID) and the research project (10062327) funded by the Ministry of Trade, Industry and Energy of Korea, Republic of.

References

[1] Keennon, Matthew, Karl Klingebiel, and Henry Won. "Development of the nano hummingbird: A tailless flapping wing micro air vehicle." 50th AIAA aerospace sciences meeting including the new horizons forum and aerospace exposition. 2012.

[2] Ma, Kevin Y., et al. "Controlled flight of a biologically inspired, insect-scale robot." Science 340.6132 (2013): 603-607.

[3] Deng, Xinyan, et al. "Flapping flight for biomimetic robotic insects: Part I-system modeling." IEEE Transactions on Robotics 22.4 (2006): 776-788.

[4] Fuller, Sawyer B., et al. "Controlling free flight of a robotic fly using an onboard vision sensor inspired by insect ocelli." Journal of The Royal Society Interface 11.97 (2014): 20140281.

[5] Loh, Kum Hoe, and Mike Cook. "Flight Dynamic Modelling and Control System Design for a Flapping Wing Micro Aerial Vehicle at Hover." AIAA Atmospheric Flight Mechanics Conference and Exhibit. 2003.

[6] Lewitowicz, Jerzy, et al. "Modeling and Simulation of Flapping Wings Microaerial-vehicles Flight Dynamics." 26th International Congress of the Aeronautical Sciences (ICAS), Anchorage, AK. 2008.

[7] Cheng, B., and X. Deng. "Near-hover dynamics and attitude stabilization of an insect model." American Control Conference (ACC), 2010. IEEE, 2010.

[8] Ohishi, Kiyoshi, et al. "Microprocessor-controlled DC motor for load-insensitive position servo system." IEEE Transactions on Industrial Electronics 1 (1987): 44-49.

[9] Lehmann, Fritz-Olaf, and Simon Pick. "The aerodynamic benefit of wingwing interaction depends on stroke trajectory in flapping insect wings." Journal of experimental biology 210.8 (2007): 1362-1377.

[10] Dickinson, Michael H., Fritz-Olaf Lehmann, and Sanjay P. Sane. "Wing rotation and the aerodynamic basis of insect flight." Science 284.5422 (1999): 1954-1960.

[11] Sane, Sanjay P., and Michael H. Dickinson. "The aerodynamic effects of wing rotation and a revised quasi-steady model of flapping flight." Journal of experimental biology 205.8 (2002): 1087-1096.

[12] Cheng, Bo, et al. "Turning dynamics and passive damping in flapping flight." Robotics and Automation, 2009. ICRA'09. IEEE International Conference on. IEEE, 2009.

[13] Nelson, Robert C. Flight stability and automatic control. Vol. 2. New York: WCB/McGraw Hill, 1998.

[14] Cheng, B., et al. "Aerodynamic damping during rapid flight maneuvers in the fruit fly Drosophila." Journal of Experimental Biology 213.4 (2010): 602-612.

[15] Finio, Benjamin M., and Robert J. Wood. "Open-loop roll, pitch and yaw torques for a robotic bee." Intelligent Robots and Systems (IROS), 2012 IEEE/RSJ International Conference on. IEEE, 2012.

[16] Kim, Joong-Kwan, and Jae-Hung Han. "Control effectiveness analysis of the hawkmoth Manduca sexta: a multibody dynamics approach." International Journal Aeronautical and Space Sciences 14.2 (2013): 152-161.

[17] Shim, Hyungbo, et al. "Yet another tutorial of disturbance observer: robust stabilization and recovery of nominal performance." Control Theory and Technology 14.3 (2016): 237-249.

[18] Li, Shihua, et al. Disturbance observer-based control: methods and applications. CRC press, 2016.

[19] Karsek, M., and A. Preumont. "Simulation of flight control of a hummingbird like robot near hover." Engineering Mechanics (2012): 322.

APPENDIX A: INERTIA COEFFICIENT

$$
\begin{aligned}
C_1 &= \frac{(I_y - I_z)I_z - I_{xz}^2}{I_x I_z - I_{xz}^2} \\
C_2 &= \frac{(I_x - I_y + I_z)I_{xz}}{I_x I_z - I_{xz}^2} \\
C_3 &= \frac{I_z}{I_x I_z - I_{xz}^2} \\
C_4 &= \frac{I_{xz}}{I_x I_z - I_{xz}^2} \\
C_5 &= \frac{I_z - I_x}{I_y} \\
C_6 &= \frac{I_{xz}}{I_y} \\
C_7 &= \frac{1}{I_y} \\
C_8 &= \frac{I_x(I_x - I_y) + I_{xz}^2}{I_x I_z - I_{xz}^2} \\
C_9 &= \frac{I_x}{I_x I_z - I_{xz}^2}
\end{aligned}
\tag{29}
$$

where I_x, I_y and I_z denotes moments of inertia with respect to the center of gravity location in the body fram.